

University of Texas Rio Grande Valley

ScholarWorks @ UTRGV

School of Earth, Environmental, and Marine
Sciences Faculty Publications and
Presentations

College of Sciences

6-13-2022

Quantitative relationships between river and channel-belt planform patterns

Tian Y. Dong

Timothy A. Goudge

Follow this and additional works at: https://scholarworks.utrgv.edu/eems_fac



Part of the [Earth Sciences Commons](#), [Environmental Sciences Commons](#), and the [Marine Biology Commons](#)

Quantitative relationships between river and channel-belt planform patterns

Tian Y. Dong¹ and Timothy A. Goudge^{1,2}

¹Jackson School of Geosciences, University of Texas at Austin, Austin, Texas 78712, USA

²CIFAR Azrieli Global Scholars Program, CIFAR, Toronto, Ontario, Canada

ABSTRACT

Channel planform patterns arise from internal dynamics of sediment transport and fluid flow in rivers and are affected by external controls such as valley confinement. Understanding whether these channel patterns are preserved in the rock record has critical implications for our ability to constrain past environmental conditions. Rivers are preserved as channel belts, which are one of the most ubiquitous and accessible parts of the sedimentary record, yet the relationship between river and channel-belt planform patterns remains unquantified. We analyzed planform patterns of rivers and channel belts from 30 systems globally. Channel patterns were classified using a graph theory-based metric, the Entropic Braided Index (eBI), which quantifies the number of river channels by considering the partitioning of water and sediment discharge. We find that, after normalizing by river size, channel-belt width and wavelength, amplitude, and curvature of the belt edges decrease with increasing river channel number (eBI). Active flow in single-channel rivers occupies as little as 1% of the channel belt, while in multichannel rivers it can occupy >50% of the channel belt. Moreover, we find that channel patterns lie along a continuum of channel numbers. Our findings have implications for studies on river and floodplain interaction, storage timescales of floodplain sediment, and paleoenvironmental reconstruction.

INTRODUCTION

Rivers display a diverse set of planform channel patterns on planetary surfaces, which are typified by meandering and braided morphologies (Leopold and Wolman, 1960). These patterns emerge from internal dynamics of sediment transport and fluid flow and external controls such as vegetation cover and confinement (Parker, 1976; Limaye and Lamb, 2013; Naito and Parker, 2020). Thus, channel patterns—if preserved in, and accurately interpreted from, the rock record—have the possibility of recording crucial paleoenvironmental information through a planet's history, helping to constrain the past climate, carbon cycling, and habitability (e.g., Ganti et al., 2019).

Through channel migration and avulsion, rivers move laterally away from their present courses. Over time, this movement forms channel belts as the amalgamation of many river courses, recording environmental signals in the stratigraphy (Hajek and Straub, 2017). In planform view, channel-belt deposits (a widely

accessible sedimentary record across planets) are observed via a range of imaging techniques, such as seismic, hyperspectral, and lidar (e.g., Cardenas et al., 2018; Durkin et al., 2018; Hayden et al., 2019; Zaki et al., 2021). Channel-belt geometries may thus provide readily accessible constraints for paleoenvironmental reconstructions. Previous work has established an empirical relationship between channel-belt width and the thickness of channel deposits (Gibling, 2006). Results of numerical and physical experiments also suggest that channel-belt width grows logarithmically, while the growth rate and stable width are sensitive to internal and external controls, such as water discharge and regional slope (Howard, 1996; Jobe et al., 2016; Limaye, 2020).

However, empirical relationships between river and channel-belt planform patterns remain elusive. Previous work on channel belts has often studied single-channel and multichannel rivers separately (Limaye, 2020; Yan et al., 2021), while in nature, planform channel pat-

terns are unlikely to conform to this binary classification (Galeazzi et al., 2021). Furthermore, while morphodynamic models have the capacity to allow rivers to self-form channel patterns, computation costs prevent these models from simulating deposits over geologic timescales (Nicholas, 2013). We explored the connections between river and channel-belt planform patterns across a range of natural systems. We hypothesize that for multichannel rivers, the ratio of channel belt to channel width will approach unity, while for single-channel rivers this ratio will greatly exceed unity (Fig. 1A). To test our hypothesis, we conducted remote sensing analysis on 30 river reaches globally (see Fig. S1 in the Supplemental Material¹). Results of this study inform future work on the interactions between rivers and their deposits, storage timescales of floodplain material, and paleoenvironmental reconstruction.

METHODS

Measuring Channel-Belt Planform Patterns

To study channel-belt planform patterns, we mapped 30 river reaches globally, spanning a range of scales and hydrology (see the Supplemental Material for detail). The main remotely sensed data sets used for mapping include European Space Agency Sentinel-2 hyperspectral images and the National Aeronautics and Space Administration Shuttle Radar Topography Mission digital elevation model. Using these data, channel-belt edges were mapped manually in ArcGIS based on changes in topography, ground texture, and vegetation (see the Supplemental Material for detail). For example, channel-belt edges are delineated using elevation difference between the inferred alluvial channel belt and terraces (Fig. 1B), ground texture differences between regions with and without abundant

¹Supplemental Material. Quantitative relationships between river and channel-belt planform patterns. Please visit <https://doi.org/10.1130/G49935.1> to access the supplemental material, and contact editing@geosociety.org with any questions.

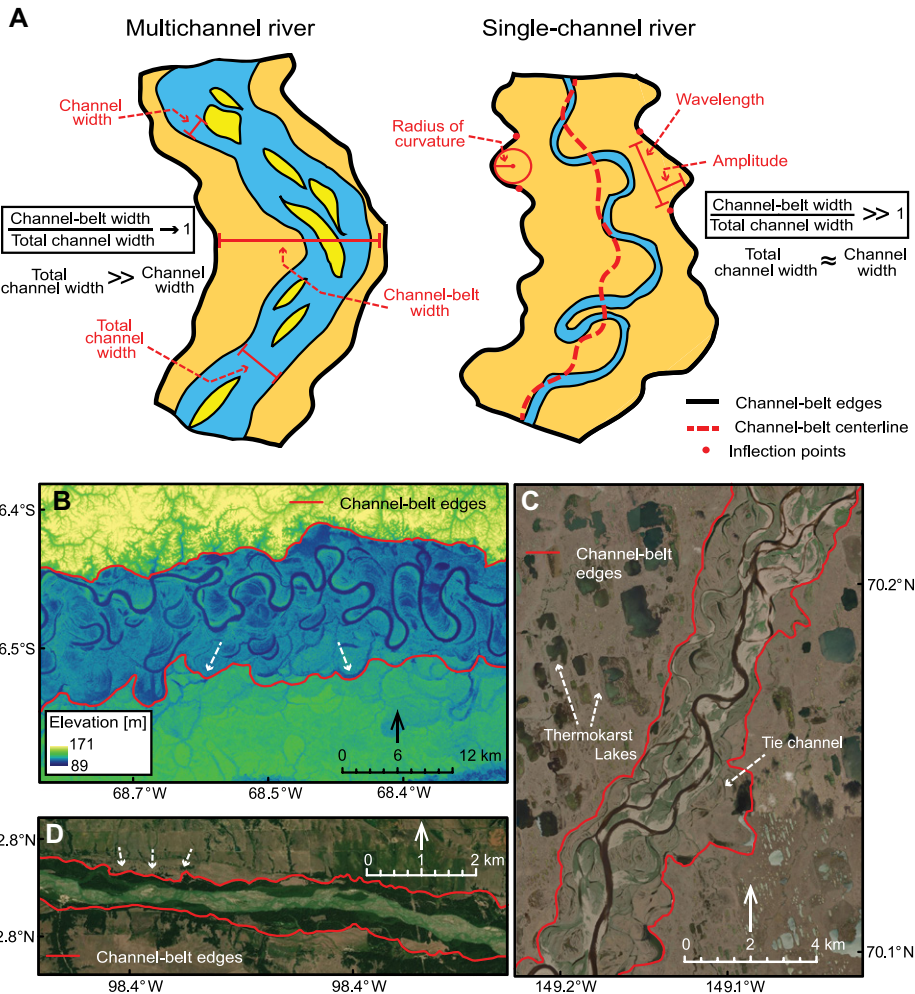


Figure 1. (A) Cartoon showing two end member cases of river and channel-belt planform patterns: (left) multichannel and (right) single-channel systems. Four planform channel-belt metrics (shown in red) are measured from the channel-belt centerline and edges: width, wavelength, amplitude, and curvature. Hypotheses are shown in black boxes. Examples of mapping channel-belt edges using (B) elevation differences at the Jurua River, Brazil, (C) ground texture at Kuparuk River, Alaska, USA, and (D) vegetation differences at Niobrara River, Nebraska, USA. White arrows indicate exemplified features for each panel.

thermokarst lakes near the channel belt (Fig. 1C), and abrupt changes in vegetation from trees/shrubs to bare earth (Fig. 1D). Channel-belt planform metrics were measured mainly using a graph theory-based mapping package called RivGraph (Schwenk and Hariharan, 2021; see the Supplemental Material for detail). A channel-belt centerline was generated automatically from the mapped belt edges (Fig. 2A). Channel-belt width was measured every ~10 m along the centerline using perpendicular transects. Three planform metrics, including wavelength, amplitude, and curvature, were measured from the channel-belt centerline and edges. These metrics were then normalized by the total active channel width to compare rivers across scales and to test our hypothesis (Fig. 1A).

Measuring Channel Planform Patterns

A binary water mask was generated for each river using a mosaic of Sentinel-2 data during

the wettest month and a modified version of the normalized difference water index (Fig. 2A; Yan et al., 2020; see the Supplemental Material for detail). The channel centerline, width, and planform patterns were extracted automatically using RivGraph from the binary mask. We quantified the channel planform pattern using the channel number calculated from the Entropic Braided Index (eBI), a method that weights each channel by the amount of water/sediment discharge it conveys (Tejedor et al., 2019; Fig. 2B):

$$eBI = 2^H. \quad (1)$$

where H is Shannon Entropy and is used to approximate the probability of a tracer particle entering a particular channel at a given cross section. Ideally, H is calculated using water/sediment discharge data, but such data at multiple cross sections along a river are scarce and challenging to collect. However, channel width

has been shown to effectively predict water and sediment discharge under steady and uniform flow conditions (Dong et al., 2020). Thus, H can be expressed in terms of channel width (b_i ; Schwenk and Hariharan, 2021):

$$H = - \sum_{i=1}^N \frac{b_i}{B} \log_2 \frac{b_i}{B}. \quad (2)$$

where i is the i th channel at a sampling cross section, N is the total number of active channels, and B is the sum of individual channel widths at the cross-section (Fig. 2B). As eBI approaches 1, most of the water and sediment discharge is conveyed in one flow path, and thus a river is considered a single-channel system. Alternatively, when eBI is much larger than 1, a river is considered a multichannel system.

RESULTS

To show the variability in our results, we report the median and interquartile ranges of the normalized channel-belt metrics and eBI along a single reach (Fig. 3A). Quantitative relationships between normalized channel-belt metrics and eBI are evaluated via linear least squares regression in logarithmic space. Note that the resulting empirical functions are used solely as a straightforward way to illustrate correlations. We find a relationship between normalized channel-belt width and eBI (Fig. 3A). In general, normalized channel-belt width decreases with increasing eBI, consistent with our hypothesis. Said another way: as eBI increases, the active river occupies a larger fraction of the channel belt. This relationship is also found after binning the data by quartiles of eBI (Fig. 3B). For the endmember cases, single-channel rivers (quartile 1, $eBI = 1.0_{-0.0}^{+0.3}$) occupy 4.3% $_{-1.1}^{+0.8}$ of the channel-belt width, while multichannel rivers (quartile 4, $eBI = 4.2_{-1.3}^{+2.1}$) occupy 27.4% $_{-7.2}^{+5.5}$ of the channel-belt width (Table S1). We also find relationships between normalized channel-belt wavelength, amplitude, and curvature, measured from both the channel-belt edges and centerline, and eBI (Fig. 4). However, metrics measured from the channel-belt centerline are nearly one order of magnitude larger than those measured from the channel-belt edges, and they have consistently lower R^2 values (Fig. 4).

DISCUSSION

Quantitative Relationships Between River and Channel-Belt Planform Patterns

We find that channel-belt width, wavelength, amplitude, and curvature, normalized by total channel width, decrease with increasing eBI (i.e., channel number). These findings indicate that channel belts, which are the amalgamation of individual river courses, retain scaling relationships with their formative channel patterns. Our results are also consistent

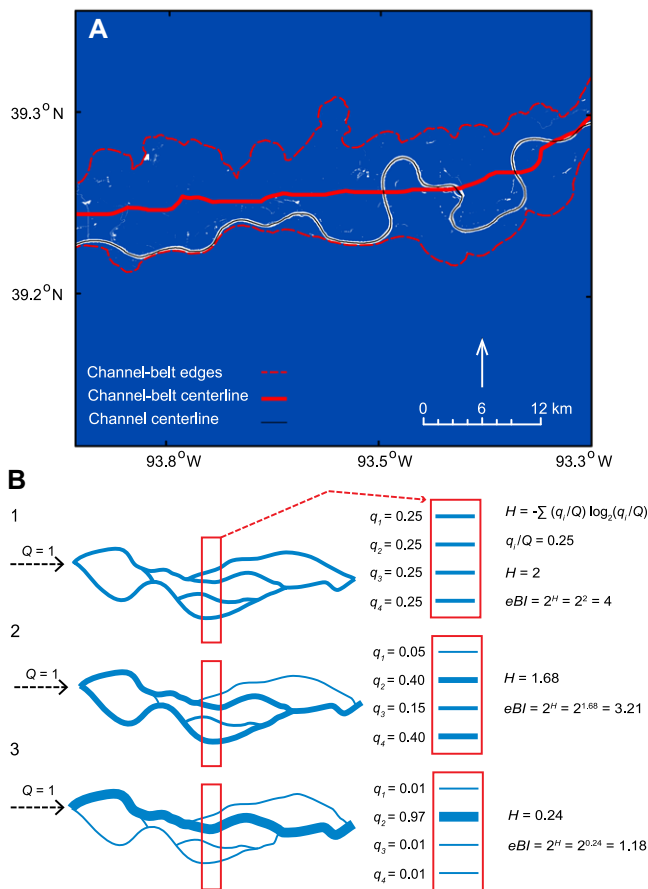


Figure 2. (A) A binary water mask generated using a modified normalized difference water index for the Missouri River, USA. (B) The concept of Entropic Braided Index is illustrated by three idealized river channel networks (after Tejedor et al., 2019). Red boxes are hypothetical survey locations.

with recent work showing similar curvature-to-width ratios for channels and channel belts (Hayden et al., 2021).

We also find that river planform patterns lie along a spectrum of channel numbers, as quantified by eBI (Figs. 3 and 4). We argue that this is intuitive, because, in essence, channel patterns are a planform expression of barforms in rivers, such that point bars are found in meandering rivers, while alternating bars are found in braided rivers (Ikeda, 1984; Sylvester et al., 2019). Theoretically, barform types are themselves well predicted by continuous hydraulic parameters, such as the Froude number, and sediment transport metrics, such as the particle Reynolds number (Ohata et al., 2017). Furthermore, because eBI measures channel number based on water and sediment discharge, this index is expected to describe channel pattern in a continuum (Tejedor et al., 2019), as shown for natural systems here (Figs. 3 and 4). Compared to previous qualitative classifications, eBI offers a more physics-based description of channel patterns (Galeazzi et al., 2021).

The linkage between barforms and channel patterns can also help explain the differences in the strength of the relationships between wavelength, amplitude, and curvature measured from channel-belt edges and the centerline (Fig. 4). Channel-belt edges are formed over time by the action of multiple river courses and thus record

the cumulative history of these rivers and their barform dimensions (Gibling, 2006). Planform metrics measured from channel-belt edges are thus expected to contain scaling relationships with channel patterns (Galeazzi et al., 2021). Conversely, the channel-belt centerline can be viewed as a long-wavelength filtered belt edge and hence is instead expected to display a muted version of information about the channel pattern. Thus, as observed, the relationships derived from the belt centerline are expected to be weaker (Fig. 4).

As eBI approaches 1 (single-channel rivers), the variability in normalized channel-belt width increases, weakening the overall quantitative relationship (Fig. 3A). We hypothesize that this increased variability is due to confinement by bedrock valleys/fluvial terraces. In confined systems, shear stress near the river banks is often insufficient to overcome the strength of the valley wall material, which limits a river's ability to expand laterally and forces water and sediment flow into a single pathway, driving incision (Larsen and Lamb, 2016). Thus, normalized channel-belt width would approach unity, even as eBI remains low (Fig. 3A). For unconfined systems, rivers can self-organize to form planform patterns based on water and sediment discharge (Parker, 1976).

To test this hypothesis, we parsed our data of normalized channel-belt width and eBI based

on confinement of the channel belt, defined as the elevation difference between the channel belt and its surrounding valley, normalized by the standard deviation of channel-belt elevation (inspired by Limaye and Lamb, 2013; see the Supplemental Material for detail). A subset of unconfined channel belts shows a stronger relationship between channel-belt width and eBI ($R^2 = 0.84$; Fig. S6B), while a subset of confined systems shows no correlation between these two metrics ($R^2 = 0.00$; Fig. S6D), which confirms our hypothesis.

As an alternative hypothesis, the observed variability in normalized channel-belt width at low eBI could also be due to age differences among the mapped river systems, where older rivers have developed a larger channel belt. However, the exact ages of mapped channel belts are unknown, and the timescale for channel-belt width to reach a stable value remains an open question. Furthermore, it is unclear why this age trend would be observed for low eBI (single-channel) rivers but not for high eBI (multichannel) rivers. Despite the causes of variability, like most geomorphic systems, channel-belt width is subject to external impacts of valley confinement while also retaining signals of internal dynamics of sediment transport and fluid flow (Parker, 1976; Hajek and Straub, 2017).

Implications for River-Channel-Belt Dynamics, Stratigraphy, and Paleoenvironmental Reconstruction

Unconfined, single-channel rivers occupy as little as 1% of the channel-belt width (Fig. 3A), implying limited interaction between the active river channel and the channel belt. While single-channel rivers migrate/avulse laterally, the timescale for a river to visit everywhere in a channel belt is on the order of centuries to millennia (Jerolmack and Mohrig, 2007), which implies that significant portions of the channel belt have limited fluvial sedimentation and thus can remain as topographic lows. Meanwhile, areas of the channel belt adjacent to the active river aggrade to become topographic highs, which promotes compensational stacking (Hajek and Straub, 2017; Jobe et al., 2020). In contrast, unconfined, multichannel systems can occupy over 50% of the channel-belt width (Fig. 3A), implying a greater interaction between the river and the channel belt. Thus, the overall deposits likely contain a greater fraction of channel deposits with smaller topographic variability, consistent with previous findings that braided systems contain more spatially connected channels in the stratigraphy (Bridge and Leeder, 1979).

Interaction between the active river and channel-belt deposits also has important implications for sediment storage timescales, which affect the terrestrial component of the organic carbon cycle. Previous studies have found that

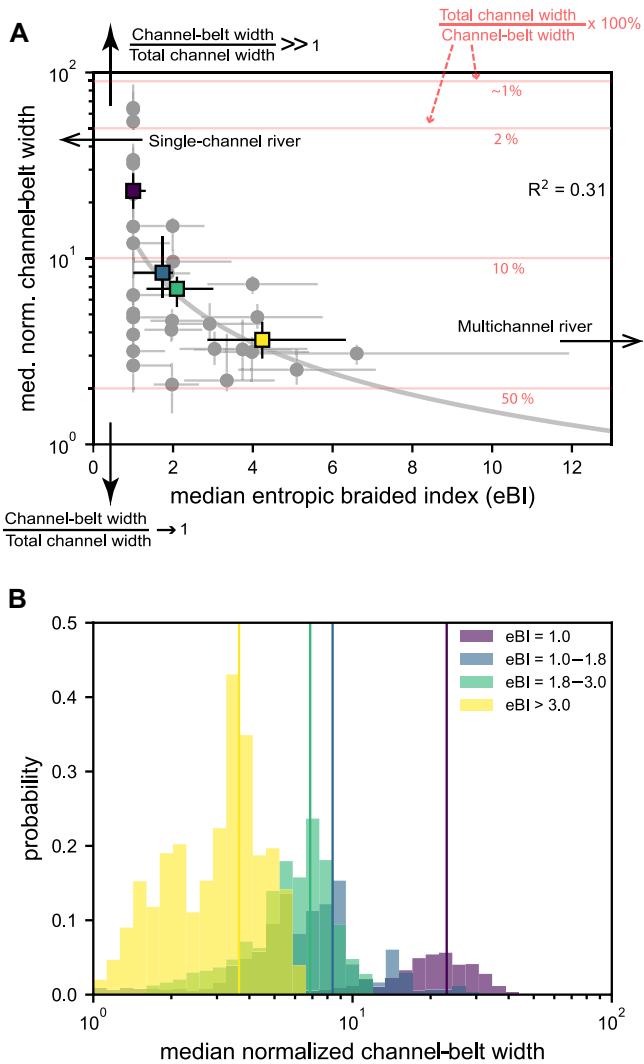


Figure 3. (A) Relationship between median normalized channel-belt width and Entropic Braided Index (eBI; Tejedor et al., 2019), shown by the gray circles. Colored squares are median values of data binned by quartiles of eBI. Error bars show interquartile range. Red lines indicate the percentage of channel-belt width occupied by the active river, which is simply the inverse of normalized channel-belt width $\times 100\%$. (B) Probability distributions of normalized channel-belt width in each quartile of eBI, which correspond to the colored squares in panel A. Vertical lines are the median.

sediment storage timescale is well described by heavy-tailed distributions in unconfined meandering rivers, and this indicates the preferential erosion of young floodplain material (e.g., Torres et al., 2017). This conclusion is consistent with our observations that indicate unconfined single-channel rivers occupy a small fraction of the channel-belt width, decreasing the probability that the active river could interact with older deposits. However, for confined or multichannel rivers, the active river occupies a much larger fraction of the channel belt, which likely reduces the age bias in fluvial erosion. It is thus reasonable to hypothesize that for these types of systems, the probability distribution of sediment storage timescale would be light tailed (Wohl, 2011; Huffman et al., 2021). In particular, confined or multichannel rivers may export a greater amount of black carbon to the ocean, affecting residence timescales of organic carbon in the ocean (Masiello, 2004).

Given the prominence of channel-belt deposits in the rock record, the relationships developed herein can be used to inform studies on past environmental changes. For example, our

findings could be readily applied to analysis of commonly observed channel-belt deposits from subsurface data (Gibling, 2006) and across Mars (Cardenas et al., 2020; Dickson et al., 2021), to reconstruct past channel patterns and environments.

ACKNOWLEDGMENTS

This material is based upon work supported by the U.S. National Science Foundation under award no. 1952814 to T. Dong. We are grateful for insightful reviews by editor William Clyde, Jason Muhlbauer, Zane Jobe, and an anonymous reviewer. T. Dong thanks C. Qiu and W. Liu for their love and support during the writing of this work. T. Dong also thanks J. Hariharan for the helpful discussion regarding the application of RivGraph.

REFERENCES CITED

Bridge, J.S., and Leeder, M.R., 1979, A simulation model of alluvial stratigraphy: *Sedimentology*, v. 26, p. 617–644, <https://doi.org/10.1111/j.1365-3091.1979.tb00935.x>.
 Cardenas, B.T., Mohrig, D., and Goudge, T.A., 2018, Fluvial stratigraphy of valley fills at Aeolis Dorsa, Mars: Evidence for base-level fluctuations controlled by a downstream water body: *Geological Society of America Bulletin*, v. 130, p. 484–498, <https://doi.org/10.1130/B31567.1>.

Cardenas, B.T., Mohrig, D., Goudge, T.A., Hughes, C.M., Levy, J.S., Swanson, T., Mason, J., and Zhao, F., 2020, The anatomy of exhumed river-channel belts: Bedform to belt-scale river kinematics of the Ruby Ranch Member, Cretaceous Cedar Mountain Formation, Utah, USA: *Sedimentology*, v. 67, p. 3655–3682, <https://doi.org/10.1111/sed.12765>.
 Dickson, J.L., Lamb, M.P., Williams, R.M.E., Hayden, A.T., and Fischer, W.W., 2021, The global distribution of depositional rivers on early Mars: *Geology*, v. 49, p. 504–509, <https://doi.org/10.1130/G48457.1>.
 Dong, T.Y., Nittrouer, J.A., McElroy, B., Il'icheva, E., Pavlov, M., Ma, H., Moodie, A.J. and Moreido, V.M., 2020, Predicting water and sediment partitioning in a delta channel network under varying discharge conditions: *Water Resources Research*, v. 56, <https://doi.org/10.1029/2020WR027199>.
 Durkin, P.R., Hubbard, S.M., Holbrook, J., and Boyd, R., 2018, Evolution of fluvial meander-belt deposits and implications for the completeness of the stratigraphic record: *Geological Society of America Bulletin*, v. 130, p. 721–739, <https://doi.org/10.1130/B31699.1>.
 Galeazzi, C.P., Almeida, R.P., and do Prado, A.H., 2021, Linking rivers to the rock record: Channel patterns and paleocurrent circular variance: *Geology*, v. 49, p. 1402–1407, <https://doi.org/10.1130/G49121.1>.
 Ganti, V., Whittaker, A.C., Lamb, M.P., and Fischer, W.W., 2019, Low-gradient, single-threaded rivers prior to greening of the continents: *Proceedings of the National Academy of Sciences of the United States of America*, v. 116, p. 11,652–11,657, <https://doi.org/10.1073/pnas.1901642116>.
 Gibling, M.R., 2006, Width and thickness of fluvial channel bodies and valley fills in the geological record: A literature compilation and classification: *Journal of Sedimentary Research*, v. 76, p. 731–770, <https://doi.org/10.2110/jsr.2006.060>.
 Hajek, E.A., and Straub, K.M., 2017, Autogenic sedimentation in clastic stratigraphy: *Annual Review of Earth and Planetary Sciences*, v. 45, p. 681–709, <https://doi.org/10.1146/annurev-earth-063016-015935>.
 Hayden, A.T., Lamb, M.P., Fischer, W.W., Ewing, R.C., McElroy, B.J., and Williams, R.M., 2019, Formation of sinuous ridges by inversion of river-channel belts in Utah, USA, with implications for Mars: *Icarus*, v. 332, p. 92–110, <https://doi.org/10.1016/j.icarus.2019.04.019>.
 Hayden, A.T., Lamb, M.P., and Carney, A.J., 2021, Similar curvature-to-width ratios for channels and channel belts: Implications for paleo-hydraulics of fluvial ridges on Mars: *Geology*, v. 49, p. 837–841, <https://doi.org/10.1130/G48370.1>.
 Howard, A.D., 1996, Modeling channel evolution and floodplain morphology, in Anderson, M.G., et al., eds., *Floodplain Processes*: Chichester, UK, Wiley, p. 15–62.
 Huffman, M.E., Pizzuto, J.E., Trampush, S.M., Moody, J.A., Schook, D.M., Gray, H.J., and Mahan, S.A., 2021, Floodplain sediment storage timescales of the laterally confined meandering Powder River, USA: *Journal of Geophysical Research: Earth Surface*, v. 127, <https://doi.org/10.1029/2021JF006313>.
 Ikeda, S., 1984, Prediction of alternate bar wavelength and height: *Journal of Hydraulic Engineering*, v. 110, p. 371–386, [https://doi.org/10.1061/\(ASCE\)0733-9429\(1984\)110:4\(371\)](https://doi.org/10.1061/(ASCE)0733-9429(1984)110:4(371)).
 Jerolmack, D.J., and Mohrig, D., 2007, Conditions for branching in depositional rivers: *Geology*, v. 35, p. 463–466, <https://doi.org/10.1130/G23308A.1>.
 Jobe, Z.R., Howes, N.C., and Auchter, N.C., 2016, Comparing submarine and fluvial channel

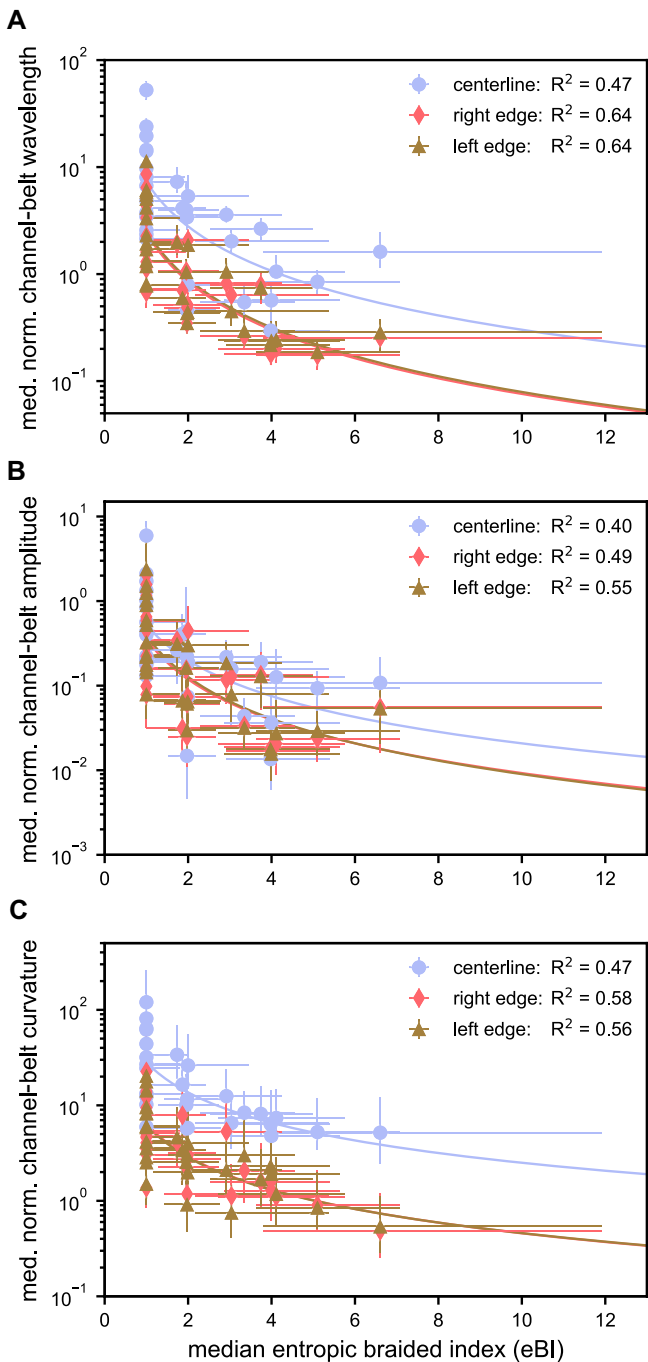


Figure 4. Relationships between median normalized, channel-belt wavelength (A), amplitude (B), and curvature (C) and Entropic Braided Index (eBI). Different symbols represent metrics measured from the channel-belt edges or centerline. Error bars show the interquartile range.

kinematics: Implications for stratigraphic architecture: *Geology*, v. 44, p. 931–934, <https://doi.org/10.1130/G38158.1>.

Jobe, Z.R., Howes, N.C., Straub, K.M., Cai, D., Deng, H., Laugier, F.J., Pettinga, L.A., and Shumaker, L.E., 2020, Comparing aggradation, super-elevation, and avulsion frequency of submarine and fluvial channels: *Frontiers of Earth Science*, v. 8, p. 53, <https://doi.org/10.3389/feart.2020.00053>.

Larsen, I.J., and Lamb, M.P., 2016, Progressive incision of the Channeled Scablands by outburst floods: *Nature*, v. 538, p. 229–232, <https://doi.org/10.1038/nature19817>.

Leopold, L.B., and Wolman, M.G., 1960, River meanders: *Geological Society of America Bulletin*, v. 71, p. 769–793, [https://doi.org/10.1130/0016-7606\(1960\)71\[769:RM\]2.0.CO;2](https://doi.org/10.1130/0016-7606(1960)71[769:RM]2.0.CO;2).

Limaye, A.B., 2020, How do braided rivers grow channel belts?: *Journal of Geophysical Research:*

Earth Surface, v. 125, <https://doi.org/10.1029/2020JF005570>.

Limaye, A.B., and Lamb, M.P., 2013, A vector-based method for bank-material tracking in coupled models of meandering and landscape evolution: *Journal of Geophysical Research: Earth Surface*, v. 118, p. 2421–2437, <https://doi.org/10.1002/2013JF002854>.

Masiello, C.A., 2004, New directions in black carbon organic geochemistry: *Marine Chemistry*, v. 92, p. 201–213, <https://doi.org/10.1016/j.marchem.2004.06.043>.

Naito, K., and Parker, G., 2020, Adjustment of self-formed bankfull channel geometry of meandering rivers: Modelling study: *Earth Surface Processes and Landforms*, v. 45, p. 3313–3322, <https://doi.org/10.1002/esp.4966>.

Nicholas, A.P., 2013, Modelling the continuum of river channel patterns: *Earth Surface Processes and Landforms*, v. 38, p. 1187–1196, <https://doi.org/10.1002/esp.3431>.

Ohata, K., Naruse, H., Yokokawa, M., and Viparelli, E., 2017, New bedform phase diagrams and discriminant functions for formative conditions of bedforms in open-channel flows: *Journal of Geophysical Research: Earth Surface*, v. 122, p. 2139–2158, <https://doi.org/10.1002/2017JF004290>.

Parker, G., 1976, On the cause and characteristic scales of meandering and braiding in rivers: *Journal of Fluid Mechanics*, v. 76, p. 457–480, <https://doi.org/10.1017/S0022112076000748>.

Schwenk, J., and Hariharan, J., 2021, RivGraph: Automatic extraction and analysis of river and delta channel network topology: *Journal of Open Source Software*, v. 6, <https://doi.org/10.21105/joss.02952>.

Sylvester, Z., Durkin, P., and Covault, J.A., 2019, High curvatures drive river meandering: *Geology*, v. 47, p. 263–266, <https://doi.org/10.1130/G45608.1>.

Tejedor, A., Schwenk, J., Kleinhans, M.G., Carling, P.A., and Fofoula-Georgiou, E., 2019, The Braiding Index 2.0: eBI: Abstract EP51E–2163 presented at 2019 Fall Meeting, American Geophysical Union, San Francisco, California, 9–13 December.

Torres, M.A., Limaye, A.B., Ganti, V., Lamb, M.P., West, A.J., and Fischer, W.W., 2017, Model predictions of long-lived storage of organic carbon in river deposits: *Earth Surface Dynamics*, v. 5, p. 711–730, <https://doi.org/10.5194/esurf-5-711-2017>.

Wohl, E., 2011, Threshold-induced complex behavior of wood in mountain streams: *Geology*, v. 39, p. 587–590, <https://doi.org/10.1130/G32105.1>.

Yan, D., Huang, C., Ma, N., and Zhang, Y., 2020, Improved Landsat-based water and snow indices for extracting lake and snow cover/glacier in the Tibetan Plateau: *Water*, v. 12, <https://doi.org/10.3390/w12051339>.

Yan, N., Colombera, L. and Mountney, N.P., 2021, Evaluation of morphodynamic controls on the preservation of fluvial meander-belt deposits: *Geophysical Research Letters*, v. 48, <https://doi.org/10.1029/2021GL094622>.

Zaki, A.S., Pain, C.F., Edgett, K.S., and Castellort, S., 2021, Global inventory of fluvial ridges on Earth and lessons applicable to Mars: *Earth-Science Reviews*, v. 216, 103561, <https://doi.org/10.1016/j.earscirev.2021.103561>.

Printed in USA